Simulation of Ultrasound Pulse Propagation in Lossy Media Obeying a Frequency Power Law

Ping He, *Member, IEEE*

***Abstract*—A method is proposed to simulate the propagation of a broadband ultrasound pulse in a lossy medium whose attenuation exhibits a power law frequency dependence. Using a bank of Gaussian filters, the broadband pulse is first decomposed into narrowband components. The effects of the attenuation and dispersion are then applied to each component based on the superposition principle. When the bandwidth of each component is narrow enough, these effects can be evaluated at the center frequency of the component, resulting in a magnitude reduction, a constant phase angle lag, and a relative time delay. The accuracy of the proposed method is tested by comparing the model-produced pulses with the experimentally measured pulses using two different phantoms. The first phantom has an attenuation function which exhibits a nearly linear frequency dependence. The second phantom has an attenuation function which exhibits a nearly quadratic frequency dependence. In deriving the dispersion from the measured attenuation, a nearly local model and a time causal model are used. For linear attenuation, the two models converge and both predict accurately the waveform of the transmitted pulse. For nonlinear attenuation, the time causal model is found more accurate than the nearly local model in predicting the waveform of the transmitted pulse.**

I. Introduction

When a broadband ultrasound pulse passes through a layer of medium, the waveform of the pulse changes as a result of the attenuation and dispersion of the medium. Many media, including soft tissues, have been observed to have an attenuation function which increases with frequency. As a result, the higher frequency components of the pulse are attenuated more than the lower frequency components. After passing through the layer, the transmitted pulse is not just a scaled down version of the incident pulse, but will have a different shape. Dispersion refers to the phenomenon that the phase velocity of a propagating wave also changes with frequency [1]. Dispersion causes additional change in the waveform of the propagating pulse because the wave components with different frequencies travel at different speeds. An understanding of the interaction of ultrasound with tissue medium in both the time and frequency domains and the ability to determine the waveform change of propagating ultrasound pulses should be valuable in the design of array transducer and in quantitative ultrasound tissue characterization [2], [3].

Manuscript received December 10, 1996; accepted July 14, 1997.

The author is with the Department of Biomedical and Human Factors Engineering, Wright State University, Dayton, OH 45435 (e-mail: phe@cs.wright.edu).

The classical method for predicting the waveform change of a signal passing through a medium relies on the impulse response of the system. According to the theory of linear systems, the output signal is the convolution of the input signal and the system's impulse response. The impulse response can be obtained by taking the inverse Fourier transform of the frequency response of the system which generally takes the following form:

$$H(\omega) = A(\omega)e^{-j\theta(\omega)x} = e^{-\alpha(\omega)x}e^{-jx\omega/V_p(\omega)} \qquad (1)$$

where $H(\omega)$ is the frequency response, $A(\omega)$ is the magnitude function, $\theta(\omega)$ is the phase angle per unit distance, $\alpha(\omega)$ is the attenuation function, $V_p(\omega)$ is the phase velocity, and x is the thickness of the layer. If $\alpha(\omega)$ and $V_p(\omega)$ are both known, the impulse response of the medium can first be synthesized and the output signal can then be determined.

The attenuation function of many soft tissues have been extensively measured and tabled [4]. In general, tissue attenuation can be expressed by a power law function [5], [6]:

$$\alpha(\omega) = \alpha_0\omega^y \qquad (2)$$

where α_0 and y are tissue-dependent attenuation parameters. On the other hand, the dispersion has been found very small and difficult to measure directly [5]. As a first approximation, one may ignore the dispersion and assume a linear-with-frequency phase term [7]. Unfortunately, the impulse response of such a system is not causal [2]. To ensure the causality while avoiding a direct measurement of the dispersion, Gurumurthy and Arthur [2] proposed a minimum-phase model for a layer of tissue. For a minimum-phase system, the attenuation and phase of its frequency response are related to each other by a pair of Hilbert transforms [8]. Because of this property, the entire frequency response, and the impulse response as well, of the layer can be obtained based on the knowledge of the medium's attenuation only. When such an approach is used to model a layer of tissue, two problems arise. First of all, the Hilbert transform relations between the attenuation and dispersion are defined in such a way that, in order to obtain the value of one of them at any single frequency, it is necessary to know the values of the other at all frequencies [2], [8]. Tissue attenuation, however, is usually measured over a limited frequency range, e.g. from 1 to 10 MHz. The first problem, therefore, is to validate the assumption that the values of α at all other frequencies can be correctly extrapolated from the measured values. The second problem is related to a so-called Paley-Wiener

condition which states that for $A(\omega)$ to be the Fourier spectrum of a causal function, a necessary and sufficient condition is that the following inequality is satisfied [8]:

$$\int_{-\infty}^{\infty} \frac{|\ln A(\omega)|}{1+\omega^2}\, dw < \infty \tag{3}$$

For most soft tissues, the attenuation function α defined in (2) is approximately a linear function of frequency ($y = 1$) [5]. Some tissues, however, have been observed to exhibit a nonlinear frequency dependence [9], [10]. In general, the exponent y for soft tissues is in the range $1 \leq y \leq 2$. For such an attenuation function, the Paley-Wiener condition is not satisfied. To overcome this problem, Gurumurthy and Arthur [2] modified the high frequency behavior of the attenuation function by imposing a high-frequency limit that beyond which the magnitude function does not go to zero faster than an exponential. Kuc [3] circumvented the problem associated with the Paley-Wiener condition by implementing the minimum phase model in the discrete-time domain. In such a case, the folding frequency (1/2 of the sampling frequency) becomes the natural high-frequency limit. The phase function between the zero and folding frequencies is derived from the attenuation function within the same frequency range by employing the Hilbert transform in the discrete-time domain. Beyond the folding frequency, however, it is assumed that the magnitude function is mirror symmetric with respect to the folding frequency (i.e., the attenuation function decreases with frequency and reaches zero at the sampling frequency) so that the impulse response is a real function. While both approaches avoid the problem associated with the Paley-Wiener condition, the assumption made on the attenuation function in a certain frequency range remains to be validated.

In this paper, we present an alternative method for determining the output signal that does not invoke the impulse response of the system and does not need the assumption about the attenuation beyond a certain frequency. The method is based on the superposition principle for a linear system: if we consider the input signal as a combination of many narrowband components, each propagating in the medium at a certain speed (dispersion) and subjecting to a frequency-dependent attenuation, the output signal can then be obtained by regrouping the individually transmitted components. In implementing the method, the attenuation is measured over the frequency range of the input signal, and the dispersion is derived from the measured attenuation over the same frequency range. In determining the dispersion from the attenuation, two models are used. The first model, which was derived by O'Donnell *et al.* [11], does not explicitly emphasize the dependence of the degree of dispersion on the exponent y in (2). The second model was proposed by Szabo [12], [13] more recently. According to Szabo's model, the degree of dispersion is strongly dependent upon the exponent y: when $y = 1$, the dispersion is maximized; when y approaches 2, the dispersion vanishes. The accuracy of the proposed method will be tested by comparing the model-produced pulses with the experimentally measured pulses using two different phantoms. The first phantom has an attenuation function which exhibits a nearly linear frequency dependence. The second phantom has an attenuation function which exhibits a nearly quadratic frequency dependence. Because the two models used to derive the dispersion from attenuation deviate from each other when $y > 1$, the transmitted waveforms predicted by the two models are expected to show noticeable difference for the second phantom. By comparing the measured and predicted waveforms, the relative accuracy of the two models also can be tested.

II. Method

A. Decomposition of a Broadband Pulse

Biological tissues appear to respond linearly to diagnostic ultrasound [2]. For such a linear system, the superposition principle holds. Consequently, the propagation of a broadband ultrasound pulse can be studied by first decomposing the pulse into many wave components, and then analyzing the propagation of each wave component. There are different ways to decompose a signal. Classical Fourier transform decomposes a signal into sinusoidal waveforms, each having a single frequency and oscillating forever. Modern wavelet analysis decomposes a signal into a set of wavelet components by dilating and translating a mother wavelet. Wavelet analysis is more efficient than Fourier analysis when the signal is dominated by transient behavior or discontinuities. Because the ultrasound pulses typically used in B-scan imaging are relatively smooth, we choose to use a simpler time-frequency representation in that each wave component will have a finite constant bandwidth which is narrow enough so that the attenuation and dispersion can be evaluated at a single frequency.

Fig. 1 shows the method of pulse decomposition. In Fig. 1(a), $r(t)$ is a band-limited incident pulse whose Fourier spectrum vanishes below a lower frequency limit f_L as well as above an upper frequency limit f_H. $H(\omega)$ represents the frequency response of the system and $g(t)$ is the transmitted pulse. In Fig. 1(b), $r(t)$ is filtered by n bandpass filters. $B_i(\omega)$ represents the frequency response of ith bandpass filter, and $r_i(t)$, $i = 1, 2, \ldots, n$, are the resulted narrowband components. The two processes shown in Fig. 1(a) and (b) are equivalent if the following equation holds:

$$r(t) = \sum_{i=1}^{n} r_i(t). \tag{4}$$

To minimize the reconstruction error produced by the process of wave decomposition, we let each bandpass filter have a Gaussian magnitude function:

$$B_i(f) = \frac{1}{\sqrt{\pi}} e^{-\left(\frac{f-f_L-(i-1)B}{B}\right)^2}, \quad i = 1, 2, \ldots, n \tag{5}$$

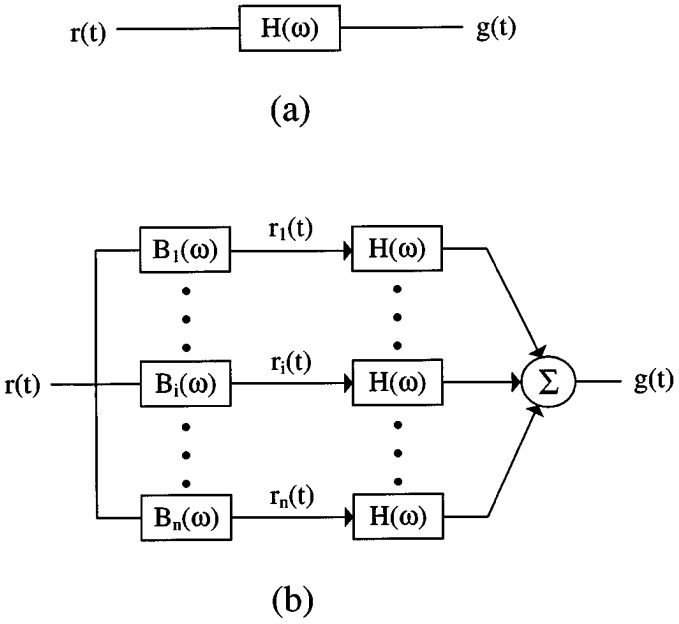

Fig. 1. (a) A broadband pulse $r(t)$ passes through a layer of medium having a frequency response of $H(\omega)$ and produces a transmitted pulse $g(t)$. (b) Based on the superposition principle, $r(t)$ is first decomposed into n narrowband components by a bank of bandpass filters. Each component $r_i(t)$ then passes through the same medium and the transmitted signals are added together to produce $g(t)$.

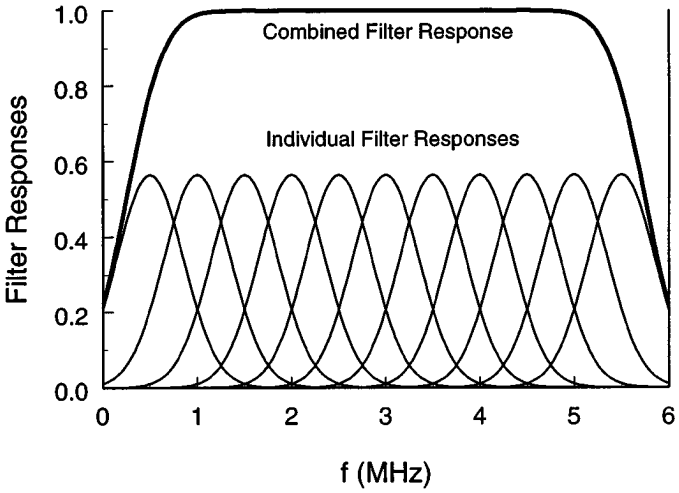

Fig. 2. Amplitude responses of the 11 bandpass filters and the combined filter response which is the summation of the 11 individual filter responses. The combined filter response has a nearly constant value of one in the midband and drops to 0.78 at 0.5 MHz and 5.5 MHz.

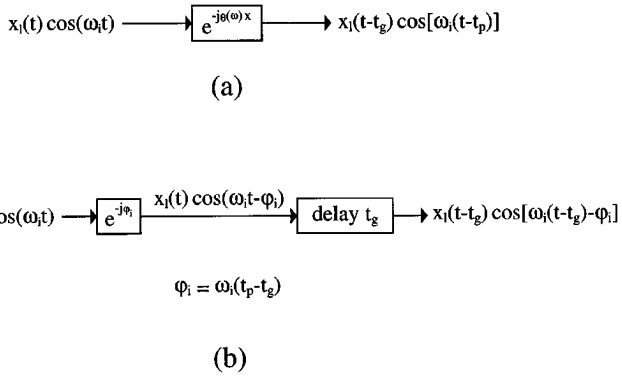

Fig. 3. (a) A modulated signal passes through a system having a unit magnitude and a phase angle of $-\theta(\omega)x$. The envelope function is delayed by a group delay t_g and the carrier is delayed by a phase delay t_p. (b) A transformed process of (a). The modulated signal now first passes through a system having a unit magnitude and a constant phase angle $-\varphi_i$. The entire waveform is then delayed by t_g. If $\varphi_i = \omega_i(t_p - t_g)$, the processes shown in (a) and (b) are equivalent.

where $B = (f_H - f_L)/(n-1)$. Fig. 2 shows the individual $B_i(f)$ of the bandpass filters which are actually used in this study. In Fig. 2, $f_L = 0.5$ MHz, $f_H = 5.5$ MHz, $n = 11$, and $B = 0.5$ MHz (the choice of n and B will be discussed later). Fig. 2 also shows that the combined filter response $\sum_i B_i(f)$ which is very close to a constant one in the midband (from 1.5 MHz to 4.5 MHz, it is within 1 ± 0.00011) and drops 2.1 dB at f_L and f_H. We will show later (in Fig. 5) that by using these Gaussian filters, the reconstruction error associated with the process of wave decomposition is negligible.

B. Transformation of the System Response

In Fig. 1, the study of the propagation of a broadband pulse through the medium is transformed into the study of the propagation of many narrowband signals through the same medium. We now use Fig. 3 to study the propagation of a particular signal, $r_i(t)$, through the medium. In Fig. 3, the narrowband signal $r_i(t)$ is represented by a modulated signal which has an envelope function $x_l(t)$ and a carrier $\cos(\omega_i t)$, where ω_i is the center frequency of $B_i(\omega)$. In addition, to concentrate on the effects of the phase term of $H(\omega)$, we temporarily drop its magnitude function (i.e., let $A(\omega) = 1$). The effects of such an $H(\omega)$ on the incident modulated signal are to impose a group delay t_g on the envelope function and a phase delay t_p on the carrier [8], where these two delays are defined as:

$$t_g = \frac{x}{V_g(\omega_i)} \quad \text{and} \quad t_p = \frac{x}{V_p(\omega_i)} \tag{6}$$

where x is the travel distance. $V_g(\omega_i)$ and $V_p(\omega_i)$ are the group and phase velocities at ω_i, respectively, which are defined as:

$$V_g(\omega_i) = \left.\frac{d\omega}{d\theta(\omega)}\right|_{\omega_i} \quad \text{and} \quad V_p(\omega_i) = \left.\frac{\omega}{\theta(\omega)}\right|_{\omega_i}. \tag{7}$$

To remove the inconvenience of imposing different delays on the envelope function and the carrier, we further transform the process shown in Fig. 3(a) to the one shown in Fig. 3(b). The modulated input signal now first passes through a filter which has a constant phase angle φ_i. The effect of this filter is to impose a phase lag φ_i on the carrier [8]. The entire waveform is then delayed by a group delay t_g. When $\varphi_i = \omega_i(t_p - t_g)$, the two processes shown in Figs. 3(a) and (b) are equivalent.

By incorporating the transforms shown in Fig. 3, the processes in Fig. 1 can then be transformed to the processes shown in Fig. 4. The constant phase delay is now

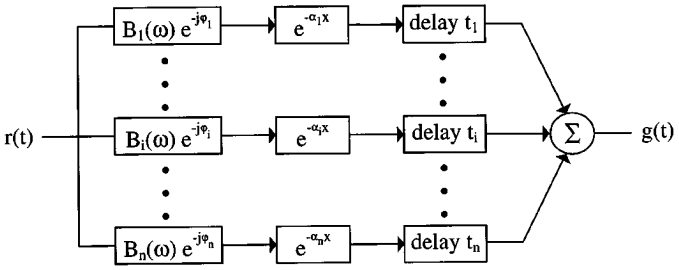

Fig. 4. The processes used to simulate the transmitted pulse $g(t)$. The incident pulse $r(t)$ first passes through n bandpass filters having a Gaussian magnitude function $B_i(\omega)$ and a constant phase angle $-\varphi_i$. Each component signal is then scaled down by an exponential factor $\exp(-\alpha_i x)$ and delayed by t_i. All component signals are then added together to produce the transmitted pulse $g(t)$.

implemented by the bandpass filter which has the same Gaussian magnitude function $B_i(\omega)$ as shown in Fig. 2, and a new phase term $e^{-j\varphi_i}$. In addition, the magnitude function, $e^{-\alpha_i x}$, of $H(\omega)$ is reinstalled, where:

$$\alpha_i = \alpha_0 \omega_i^y. \tag{8}$$

In implementing the processes shown in Fig. 4, the attenuation of the medium is actually measured. The phase delay and group delay are calculated from the measured attenuation using the two models which will be discussed in the next section.

C. Determine Phase Delay and Group Delay from Attenuation

The Hilbert transform relations between ultrasound attenuation and dispersion used by Gurumurthy and Arthur [2] and Kuc [3] can be considered as the generalized Kramers-Kronig relations which were originally derived to link the absorption and dispersion of electromagnetic waves [14]. If we use $e^{j(\omega t - Kx)}$ to represent a plane wave propagating in the x direction, where $K = \theta(\omega) - j\alpha(\omega)$ is the complex wave number, the Kramers-Kronig relations state that the real part, $\theta(\omega) = \omega/V_p(\omega)$, and the imaginary part, $\alpha(\omega)$, of K are related to each other by a pair of Hilbert transforms. Because the validity of these relations only requires that the supporting medium is passive, linear, and casual, the Kramers-Kronig relations can be applied to a wide class of homogeneous and inhomogeneous media as well as to various waves including elastic, acoustic and electromagnetic waves [15].

The literature on causality and dispersion relations is extensive [16], [17]. In this paper we will use two specific models, both enabling calculation of the dispersion from the local attenuation, that are particularly suitable to the proposed method. The first model was derived by O'Donnell *et al.* [11] and will be referred as the nearly local model. The second model was proposed by Szabo and will be referred as the time causal model [13]. Using each model, the phase delay t_p, group delay t_g, and the phase angle φ_i will be derived.

Nearly local model: By applying the Kramers-Kronig relations to a linear and causal acoustic system, and assuming that the attenuation function and phase velocity do not change rapidly over the frequency range of interest, O'Donnell *et al.* [11] derived a useful equation which enables one to calculate the phase velocity using the knowledge of local attenuation:

$$\frac{1}{V_p(\omega)} = \frac{1}{V_p(\omega_0)} - \frac{2}{\pi} \int_{\omega_0}^{\omega} \frac{\alpha(s)}{s^2}\, ds \tag{9}$$

where ω_0 is a reference frequency; $V_p(\omega)$ and $V_p(\omega_0)$ are the phase velocities at an arbitrary frequency ω and at ω_0, respectively, and α is the attenuation function. For the attenuation function obeying a power law as shown in (2), the integration in (9) needs to be evaluated separately for $y = 1$ and $y > 1$:

$$\frac{1}{V_p(\omega)} = \frac{1}{V_p(\omega_0)} - \frac{2\alpha_0}{\pi} \ln \frac{\omega}{\omega_0} \qquad \text{for } y = 1 \tag{10}$$

and

$$\frac{1}{V_p(\omega)} = \frac{1}{V_p(\omega_0)} - \frac{2\alpha_0}{\pi(y-1)} (\omega^{y-1} - \omega_0^{y-1}) \text{ for } y > 1. \tag{11}$$

To find $V_g(\omega)$, we use the relations $\theta(\omega) = \omega/V_p(\omega)$, together with (10) and (11):

$$\frac{1}{V_g(\omega)} = \frac{d\theta}{d\omega} = \frac{1}{V_p(\omega_0)} - \frac{2\alpha_0}{\pi} \left(\ln \frac{\omega}{\omega_0} + 1 \right) \text{ for } y = 1 \tag{12}$$

and

$$\frac{1}{V_g(\omega)} = \frac{1}{V_p(\omega_0)} - \frac{2\alpha_0}{\pi(y-1)} (y\omega^{y-1} - \omega_0^{y-1}) \text{ for } y > 1. \tag{13}$$

The group delay, t_i in Fig. 4 can then be obtained:

$$t_i = \frac{x}{V_g(\omega_i)} = \frac{x}{V_p(\omega_0)} - \frac{2\alpha_0 x}{\pi} \left(\ln \frac{\omega_i}{\omega_0} + 1 \right) \text{ for } y = 1 \tag{14}$$

and

$$t_i = \frac{x}{V_p(\omega_0)} - \frac{2\alpha_0 x}{\pi(y-1)} (y\omega_i^{y-1} - \omega_0^{y-1}) \qquad \text{for } y > 1 \tag{15}$$

where x is the thickness of the layer. Finally, based on Fig. 3, the phase angle φ_i can be obtained from (6) and (10)–(13):

$$\begin{aligned} \varphi_i &= \omega_i (t_p - t_g) \\ &= \omega_i \left(\frac{x}{V_p(\omega_i)} - \frac{x}{V_g(\omega_i)} \right) = \frac{2\omega_i \alpha_0 x}{\pi} \text{ for } y = 1 \end{aligned} \tag{16}$$

and

$$\varphi_i = \frac{2\omega_i^y \alpha_0 x}{\pi} \qquad \text{for } y > 1. \tag{17}$$

Time causal model: Szabo [12] derived a time domain expression of causality analogous in function to the Kramers-Kronig relations in the frequency domain. Based on this new time casual model, an equation similar to (11) was derived which enables one to calculate the phase velocity from the attenuation values near a reference frequency ω_0 [13]. The original form of equation 27 shown in Szabo's paper [13] is recasted here as:

$$\frac{1}{V_p(\omega)} = \frac{1}{V_p(\omega_0)} + \alpha_0 \tan\left(\frac{y\pi}{2}\right)(\omega^{y-1} - \omega_0^{y-1}). \tag{18}$$

By comparing (11) and (18), one finds a simple procedure to transform the results obtained by the nearly local model to the corresponding results predicted by the time casual model. That is to perform the following conversion:

$$\frac{2}{\pi(y-1)} \longrightarrow -\tan\left(\frac{y\pi}{2}\right). \tag{19}$$

When y approaches 1 from the right side ($y > 1$),

$$\frac{2}{\pi(y-1)} \cong -\tan\left(\frac{y\pi}{2}\right). \tag{20}$$

As a result, when $y = 1$, the two models converge and the time causal model will predict the same results as shown in (12), (14), and (16). When $y > 1$, the two models deviate from each other, and the time causal model predicts the following results:

$$\frac{1}{V_g(\omega)} = \frac{1}{V_p(\omega_0)} + \alpha_0 \tan\left(\frac{y\pi}{2}\right)(y\omega^{y-1} - \omega_0^{y-1}) \tag{21}$$

$$t_i = \frac{x}{V_p(\omega_0)} + \alpha_0 x \tan\left(\frac{y\pi}{2}\right)(y\omega_i^{y-1} - \omega_0^{y-1}) \tag{22}$$

$$\varphi_i = -(y-1)\omega_i^y \alpha_0 x \tan\left(\frac{y\pi}{2}\right). \tag{23}$$

III. Measurement and Simulation Results

To test the processes shown in Fig. 4 for predicting the waveform of the transmitted pulse, two phantoms are used in through-transmission measurements. The first phantom is a Plexiglas block, which has an almost linear-with-frequency attenuation. The speed of sound of the material is measured as 2736 m/s. The second phantom, which is manufactured by ATS Laboratories (Bridgeport, CT), is made of a special rubber material having a speed of sound of 1465 m/s. The ATS phantom material has an attenuation function which exhibits a highly nonlinear frequency dependence. The thickness of both phantoms is 8.0 cm.

Two transducers are situated 25 cm apart in a water tank and are aligned properly. The transmitting transducer (Panametrics V309, 13-mm aperture) has a nominal center frequency of 5.0 MHz and a focal length of 89 mm. The receiving transducer (Panametrics V382, 13-mm aperture) has a nominal center frequency of 3.5 MHz

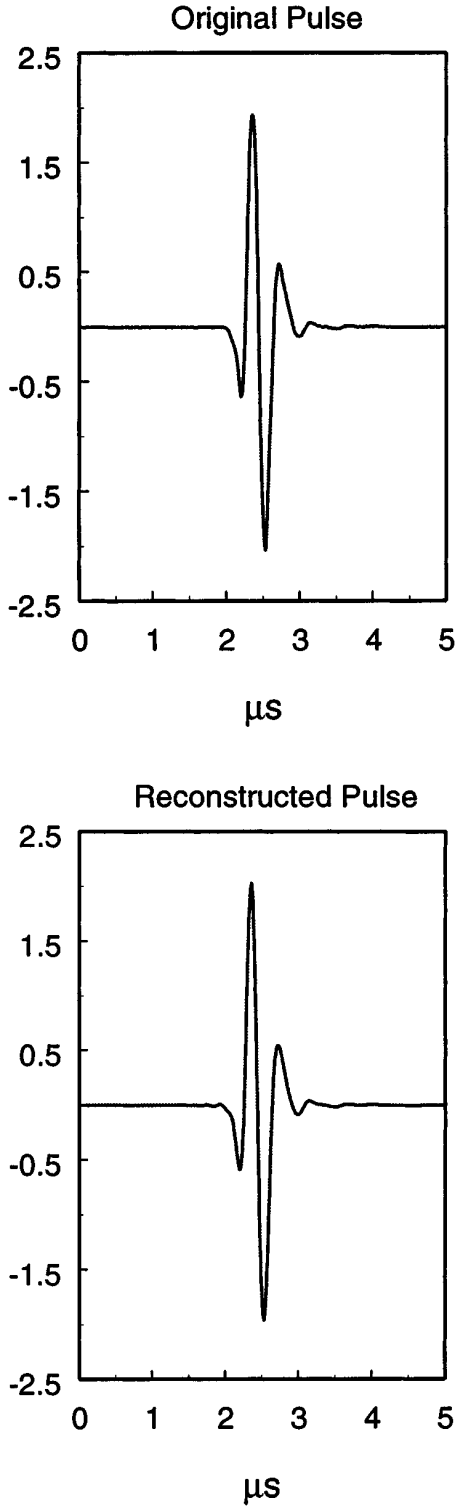

Fig. 5. The original pulse $r(t)$ and the reconstructed pulse by added together the filter-produced signals $r_i(t)$ shown in Fig. 1. Using $r(t)$ as the reference, the normalized rms error of the reconstructed pulse is 4.5%.

and a focal length of 76 mm. The pulser/receiver used in the study is Panametrics 5052PR. The RF data amplified by the receiver are digitized by a SONY/TEK 390AD programmable digitizer which has a 10-bit resolution and a sampling frequency of 60 MHz. With only a water path between the two transducers, the pulse waveform received by the receiving transducer is recorded which will be used as the incident pulse, $r(t)$, in the following processes.

By taking the Fourier transform, $r(t)$ is found to be band limited in the frequency range of 0.5 MHz to 5.5 MHz. Based on this frequency range, 11 bandpass filters are used to decompose $r(t)$ into its components (the choice of the number of bands will be discussed later). The magnitude transfer functions of these filters are expressed by (5) and plotted in Fig. 2. As a first test, we use the 11 bandpass filters as shown in Fig. 1 to decompose the incident pulse $r(t)$ and then reconstruct a pulse by adding the resulted components together according to (4). Fig. 5 compares the waveforms of the original pulse $r(t)$ and the reconstructed pulse. In these plots, as well as in the rest waveform plots, the ordinate shows only the relative magnitude without a specific unit. We now define a normalized root-mean-square (rms) error which will be used throughout this paper for pulse comparisons:

$$\overline{\varepsilon} = \frac{\sqrt{\sum_{i=1}^{N}[x(i)-x_o(i)]^2/N}}{\sqrt{\sum_{i=1}^{N}[x_o(i)]^2/N}} = \sqrt{\frac{\sum_{i=1}^{N}[x(i)-x_o(i)]^2}{\sum_{i=1}^{N}[x_o(i)]^2}} \quad (24)$$

where $x(i)$ is a sample of the signal to be tested, $x_0(i)$ is the corresponding sample of the reference signal, and N is the total number of samples. Using the original pulse $r(t)$ as the reference, the normalized rms error of the reconstructed pulse shown in Fig. 5 is 4.5%.

Fig. 6 shows the waveforms of three components which are produced by the bandpass filters with the center frequencies of 1 MHz, 3 MHz, and 5 MHz, respectively.

A. Measurement and Simulation with the Plexiglas Phantom

We then insert the Plexiglas phantom in between the transmitting and receiving transducers. The received pulse, $g_0(t)$, will be used as the reference signal against which the model-predicated pulses $g(t)$ will be compared.

If we use $R(\omega)$ and $G_0(\omega)$ to represent the amplitude spectral functions of $r(t)$ and $g_0(t)$, respectively, and assuming the attenuation of water is negligible, we obtain [18]:

$$G_o(\omega) = R(\omega)T_1T_2e^{-\alpha(\omega)x} \quad (25)$$

where T_1 and T_2 are the transmission coefficients at the water-Plexiglas interface (incident side) and at the Plexiglas-water interface (exit side), respectively, and x is the thickness of the Plexiglas block. By taking logarithm on the both sides of (25), we obtain:

$$\frac{1}{x}[\ln R(\omega) - \ln G_0(\omega)] = \frac{1}{x}\ln\left(\frac{1}{T_1T_2}\right) + \alpha_0\omega^y. \quad (26)$$

If we fit the function shown on the left side of (26) with an exponential function

$$\alpha_a(f) = b_0 + \beta f^y. \quad (27)$$

where $\alpha_a(f)$ is the apparent attenuation function, we obtain:

$$T_1T_2 = e^{-xb_0}, \text{ and } \alpha_0 = \beta(2\pi)^{-y} \quad (28)$$

α_0 and y determine the frequency-dependent attenuation and will be used to calculate the dispersion. The factor T_1T_2 is not a part of the tissue model discussed so far. This frequency-independent factor, however, causes a scaled-down of the amplitude of the transmitted pulse. In order to maintain a faithful comparison between the simulated and experimentally recorded pulses, all the simulated pulses obtained by the processes shown in Fig. 4 (i.e., $g(t)$) will be multiplied by a factor T_1T_2 before being compared with the experimental results.

The attenuation function of the Plexiglas phantom is plotted in Fig. 7. Over the frequency range of $r(t)$, the apparent attenuation is approximately a linear function of frequency ($y = 1$) with $b_0 = 0.96$ dB/cm and $\beta = 0.89$ dB/(MHz cm). T_1T_2 and α_0 can then be calculated according to (28). In implementing the processes shown in Fig. 4, 11 bandpass filters are used with center frequencies of 0.5, 1.0, 1.5, 2.0, 2.5, 3.0, 3.5, 4.0, 4.5, 5.0, and 5.5 MHz, respectively. α_i are determined by (8) and φ_i are determined by (16). To calculate t_i using (14), we choose the midband frequency, $(f_L + f_H)/2 = 3.0$ MHz, as the reference frequency (i.e., $\omega_0/2\pi$), and let $V_p(\omega_0) = 2736$ m/s. Because we are only interested in the relative delays among the component signals, we let the midband ($i = 6$, $f_c = 3.0$ MHz) have zero delay and express the delays of all other bands as the relative delays with respect to the midband. Table I lists the calculated phase angles and relative time delays based on the measured attenuation of the Plexiglas phantom. A positive delay means that the component signal of the particular band travels slower than that of the reference band (midband) and a negative delay means a faster traveling speed. As indicated by Table I, the Plexiglas has an anomalous dispersion [2]: the signal having a higher center frequency travels faster than the one having a lower center frequency. To reconstruct the transmitted pulse $g(t)$, the signal of the midband is not changed, while the signals of all other bands are either shifted backward (for positive delay) or forward (for negative delay) with respect to the reference signal, according to the calculated relative delays. The shifted signals are then added together to produce the transmitted pulse $g(t)$.

Fig. 8 compares the simulated pulses with the measured one. The pulse shown in Fig. 8(a) is the transmitted pulse $g_0(t)$ which is experimentally measured. Fig. 8(b) shows

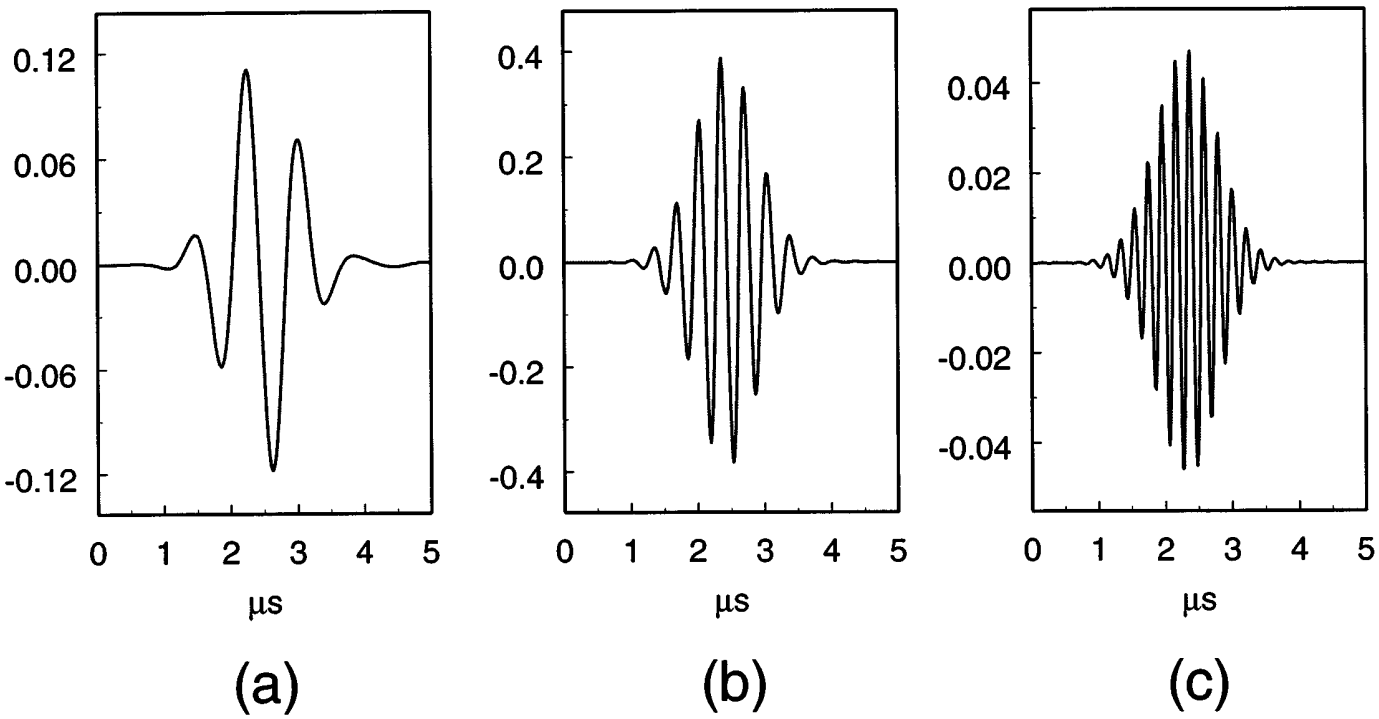

Fig. 6. Waveforms of three component signals produced by the bandpass filters having center frequencies of (a) 1 MHz, (b) 3 MHz, and (c) 5 MHz.

TABLE I
PHASE ANGLES AND RELATIVE TIME DELAYS OF THE 11 BANDS USED TO PRODUCE THE TRANSMITTED PULSE SHOWN IN FIG. 8(B). THESE PARAMETERS ARE DERIVED FROM THE ATTENUATION FUNCTION OF THE PLEXIGLAS PHANTOM SHOWN IN FIG. 7.

Band number	φ (radians)	Delay ($\times 10^{-7}$ s)
1	0.261	1.489
2	0.522	0.912
3	0.783	0.576
4	1.044	0.337
5	1.305	0.151
6	1.566	0.000
7	1.827	−0.128
8	2.087	−0.239
9	2.347	−0.337
10	2.609	−0.424
11	2.870	−0.503

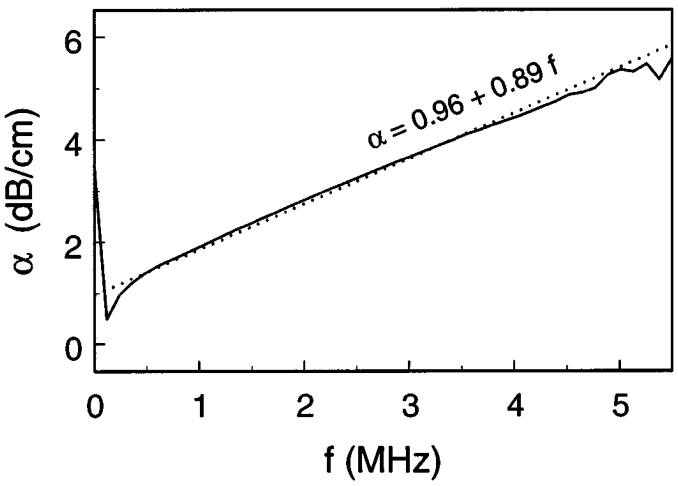

Fig. 7. Attenuation function of the Plexiglas phantom. Over the frequency range of 0.5 to 5.5 MHz, the attenuation function is fitted by a straight line $\alpha = 0.96 + 0.89$ f.

the transmitted pulse $g(t)$ simulated using the processes shown in Fig. 4 and the parameters listed in Table I. The pulse shown in Fig. 8(c) is produced by a nondispersive model, i.e., by a filter with linear-phase or zero-phase [7]. This pulse is obtained by letting all φ_i and t_i in Fig. 4 be zero. As indicated by Fig. 8, the simulated pulse in Fig. 8(b) bears a closer resemblance to the measured pulse in Fig. 8(a) than the pulse in Fig. 8(c) does. Using the pulse in Fig. 8(a) as the reference, the normalized rms error of the pulse in Fig. 8(b) is 6.8% and the normalized rms error of the pulse in Fig. 8(c) is 35.7%. To minimize the rms error, the pulses in Figs. 8(b) and (c) are allowed to be shifted left and right to achieve a best alignment with the pulse in Fig. 8(a). On the other hand, no adjustment has been made to the magnitude of each pulse.

B. Measurement and Simulation with the ATS Phantom

Fig. 9 shows the attenuation function obtained from the ATS phantom. Because the fitted curve shows a value of $y = 1.98$, we shall expect a difference between the results predicted by the nearly local model and the time causal model. From the attenuation parameters obtained from the fitted curve, T_1T_2, α_0, and y are first deter-

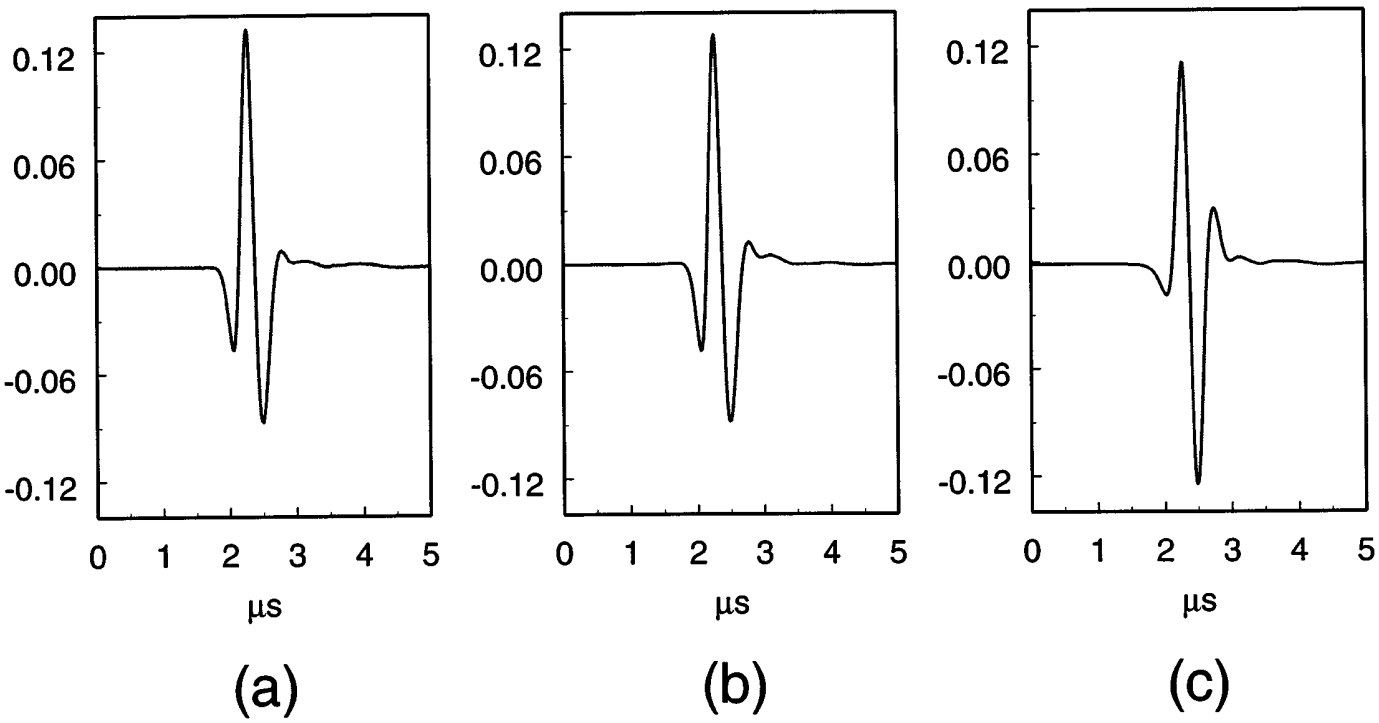

Fig. 8. (a) Experimentally measured pulse by passing $r(t)$ through the Plexiglas phantom. (b) Simulated pulse using the processes shown in Fig. 4. The normalized rms error is 6.8%. (c) Simulated pulse using a zero-phase filter. The normalized rms error is 35.7%.

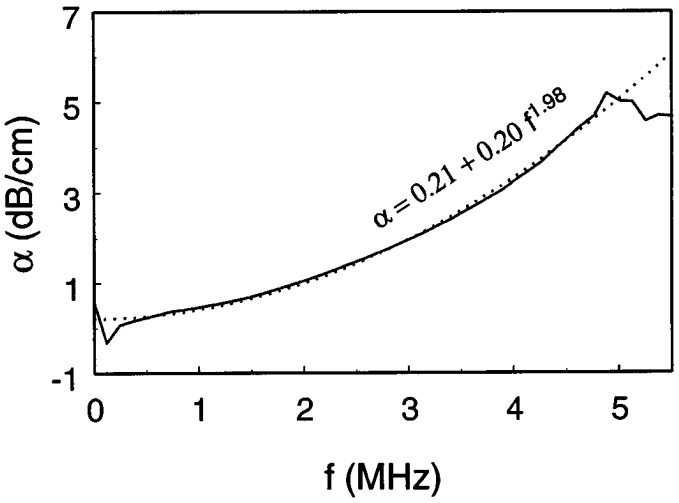

Fig. 9. Attenuation function of the ATS phantom. Over the frequency range of 0.5 to 5.5 MHz, the attenuation function is fitted by a curve $\alpha = 0.21 + 0.20\ \mathrm{f}^{1.98}$.

TABLE II
PHASE ANGLES AND RELATIVE TIME DELAYS OF THE 11 BANDS USED TO PRODUCE THE TRANSMITTED PULSES SHOWN IN FIG. 10(B) AND (C). THESE PARAMETERS ARE DERIVED FROM THE ATTENUATION FUNCTION OF THE ATS PHANTOM SHOWN IN FIG. 9 BASED ON THE TIME CASUAL MODEL AND THE NEARLY LOCAL MODEL, RESPECTIVELY.

Band number	Time-causal model φ (radians)	Time-causal model Delay ($\times 10^{-7}$ s)	Nearly-local model φ (radians)	Nearly-local model Delay ($\times 10^{-7}$ s)
1	0.001	0.044	0.030	0.915
2	0.006	0.035	0.117	0.730
3	0.013	0.026	0.262	0.546
4	0.022	0.018	0.463	0.363
5	0.035	0.009	0.720	0.181
6	0.050	0.000	1.033	0.000
7	0.068	−0.009	1.401	−0.180
8	0.088	−0.017	1.825	−0.360
9	0.112	−0.026	2.304	−0.540
10	0.137	−0.035	2.839	−0.719
11	0.166	−0.043	3.429	−0.898

mined using (27) and (28), and α_i for the 11 bands are then determined by (8). For the nearly local model, φ_i are calculated by (17), and t_i are determined by (15) with $V_p(\omega_0) = 1465$ m/s. For the time causal model, φ_i are calculated by (23), and t_i are determined by (22). The resulted phase angles and relative time delays for the two models are listed in Table II. As one would expect, the values of both parameters of the time casual model are much smaller than that of the nearly local model.

Fig. 10 compares the simulated transmitted pulses using the two models with the measured pulse. The pulse shown in Fig. 10(a) is the transmitted pulse measured experimentally. The pulse shown in Fig. 10(b) is the simulated pulse using the time casual model. Using the pulse in Fig. 10(a) as the reference, the normalized rms error of the pulse in Fig. 10(b) is 6.2%. The pulse shown in Fig. 10(c) is the simulated pulse using the nearly local model. The normalized rms error of this pulse is 30.9%.

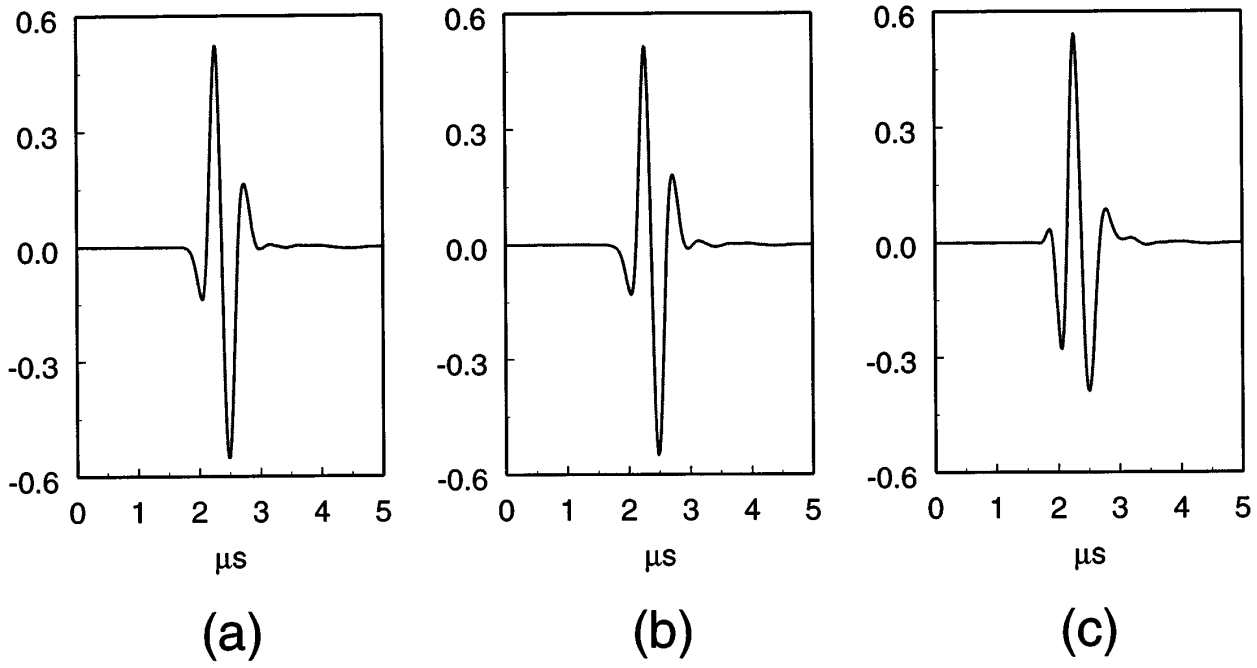

Fig. 10. (a) Experimentally measured pulse by passing $r(t)$ through the ATS phantom. (b) Simulated pulse using the time causal model. The normalized rms error is 6.2%. (c) Simulated pulse using the nearly local model. The normalized rms error is 30.9%.

C. Measurement and Simulation Using a Narrowband Transducer

The same experiments and simulations are repeated by replacing the transmitting transducer (Panametrics V309) with another transducer (Panametrics A382, 13-mm aperture, 76 mm focal length) which has a narrower bandwidth. For the new incident pulse $r(t)$, we choose $f_L = 1.5$ MHz, $f_H = 4.5$ MHz, and a total of 7 frequency bands with the following center frequencies: 1.5, 2.0, 2.5, 3.0, 3.5, 4.0, and 4.5 MHz.

Fig. 11 compares the simulated pulses with the measured one using the Plexiglas phantom. Again, the pulse shown in Fig. 11(a) is the experimentally recorded one. The pulse shown in Fig. 11(b) is predicted by the dispersive model using (8), (14), and (16). Using the pulse in Fig. 11(a) as the reference, the normalized rms error of the pulse in Fig. 11(b) is 5.7%. The pulse in Fig. 11(c) is predicted by a nondispersive model. The normalized rms error is 20.3%.

Fig. 12 compares the simulated pulses with the measured one using the ATS phantom. The pulse in Fig. 12(a) is the measured transmitted pulse. The pulse shown in Fig. 12(b) is predicted by the time causal model. Using the pulse in Fig. 12(a) as the reference, the normalized rms error of the pulse in Fig. 12(b) is 8.8%. The pulse in Fig. 12(c) is predicted by the nearly local model. The normalized rms error of the pulse in Fig. 12(c) is 21.1%.

IV. Discussion

A method to simulate the propagation of a broadband ultrasound pulse in a lossy and dispersive medium is presented. The method uses a time-frequency representation in that the original broadband pulse is decomposed into narrowband components which are localized in both the time and frequency domains. This approach is similar to the one used by Önsay and Haddow [19] who studied the propagation of impact-induced bending waves along a uniform beam using the wavelet transform analysis. The method used in this paper is different from the typical wavelet analysis in that the components are produced by a set of bandpass filters having a constant bandwidth, rather than by dilating and translating a mother wavelet [19]. In addition, the inverse transform is not needed in the proposed method. This simplification is achieved by choosing a bank of special Gaussian filters as shown in Fig. 2. As a result, the original pulse is a direct summation of the narrowband components as indicated by (4).

In addition to satisfying (4), the validity of the proposed method requires that the bandwidth of each component is narrow enough so that the effects of the attenuation and dispersion can be evaluated at a single frequency—the center frequency of the component signal, as indicated in Fig. 4. We now determine the criterion for the bandwidth of each component to be narrow enough, i.e., to determine an upper limit for B in (5). It is well-known that, when a pulse with a finite bandwidth propagating in a lossy medium, its mean frequency will be shifted down and, therefore, deviate from the original mean frequency. The amount of downshift is related to the bandwidth of the pulse: a wider bandwidth will produce a more significant downshift in the mean frequency. Based on this consideration, the narrowband criterion may be defined as to find an upper limit for B so that the resulted downshift in the mean frequency will be negligible.

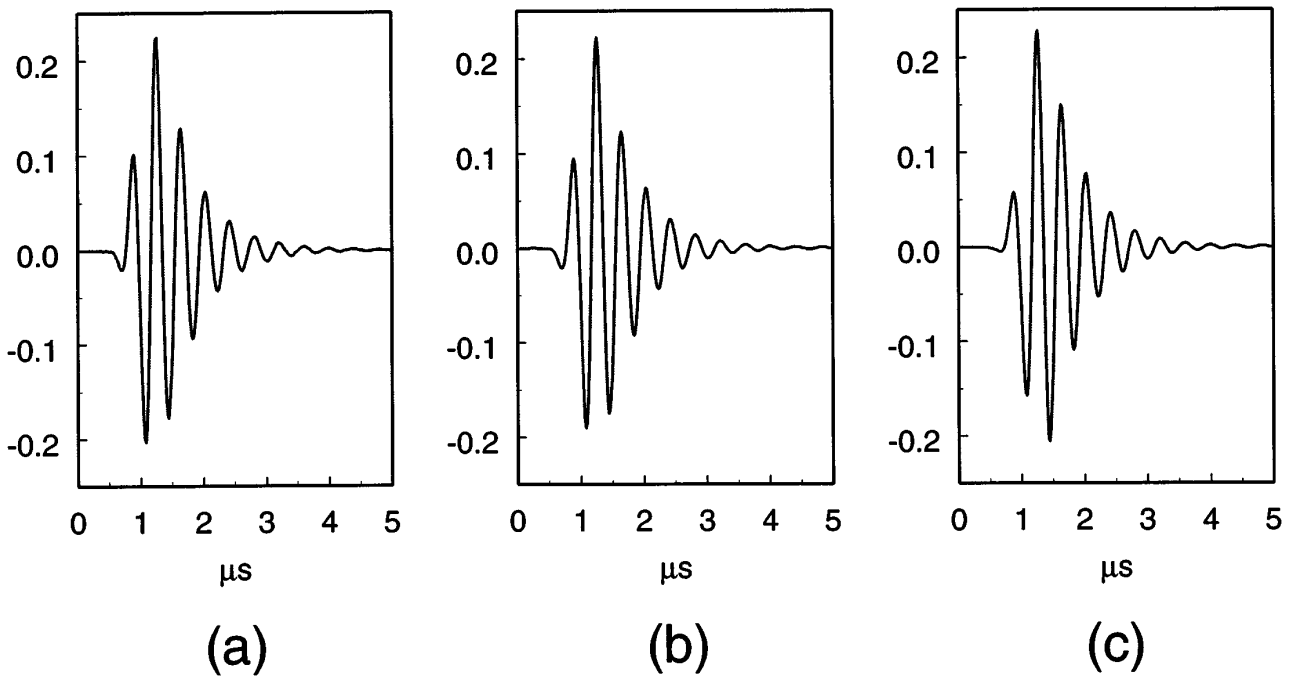

Fig. 11. (a) Experimentally measured pulse by passing a narrowband pulse through the Plexiglas phantom. (b) Simulated pulse using the processes shown in Fig. 4. The normalized rms error is 5.7%. (c) Simulated pulse using a zero-phase filter. The normalized rms error is 20.3%.

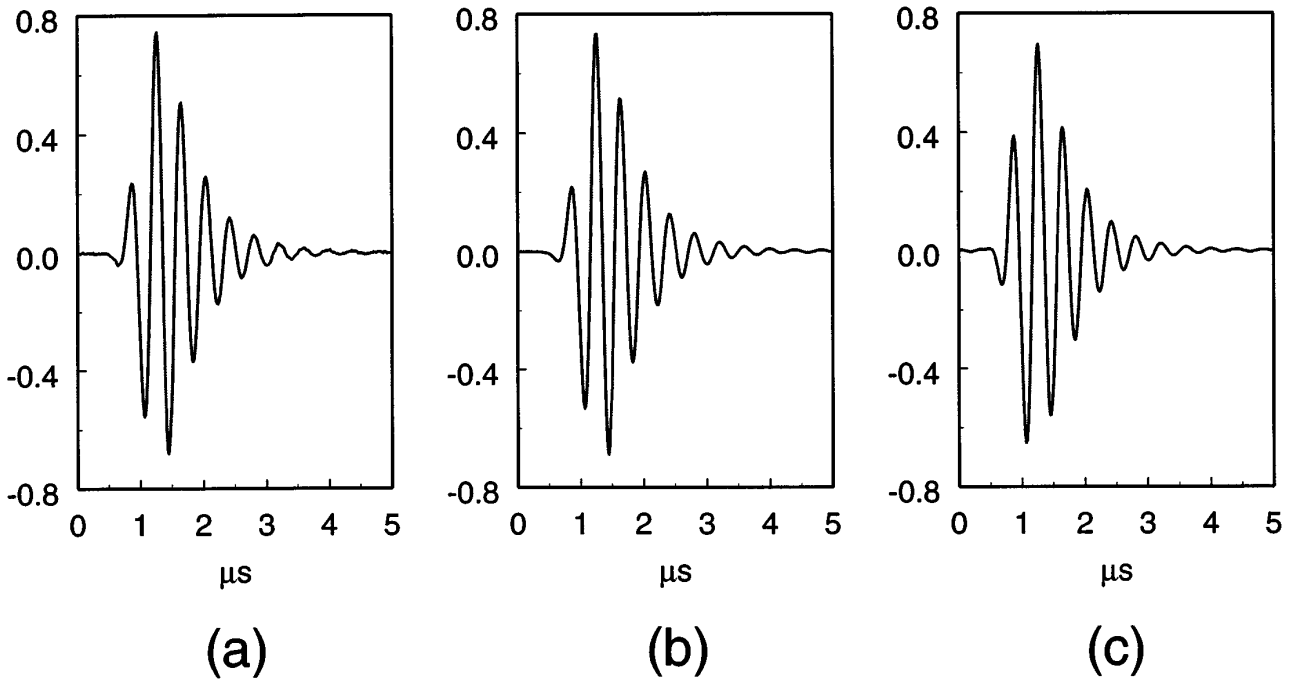

Fig. 12. (a) Experimentally measured pulse by passing the same pulse used in Fig. 11 through the ATS phantom. (b) Simulated pulse using the time causal model. The normalized rms error is 8.8%. (c) Simulated pulse using the nearly local model. The normalized rms error is 21.1%.

Let us consider a particular component in Fig. 4 which has a center frequency of f_c. Because the component is produced by passing a broadband $r(t)$ through a narrow bandpass filter having a Gaussian spectrum, the spectrum of the resulted component is also approximately a Gaussian function:

$$S_0(f) = Ae^{-\frac{(f-f_c)^2}{B^2}} \tag{29}$$

where A is the amplitude of $S_0(f)$ at the center frequency f_c, and B is the same bandwidth parameter of $B_i(f)$ in (5). After passing through a tissue layer having an attenuation function $\alpha(f) = \beta f^y$ and a thickness x, the spectrum of the attenuated pulse becomes:

$$S_1(f) = Ae^{-\frac{(f-f_c)^2}{B^2}} e^{-\beta f^y x}. \tag{30}$$

We now consider the two extreme cases: $y = 1$ and $y = 2$. For $y = 1$, it can be shown that:

$$S_1(f) = \overline{A} e^{-\frac{(f-\overline{f_c})^2}{B^2}} \tag{31}$$

where $\overline{A}$ is the new amplitude which is independent of frequency, and $\overline{f_c}$ is the down-shifted new center frequency:

$$\overline{f_c} = f_c - \frac{\beta B^2 x}{2}. \tag{32}$$

We may then require that the relative down-shift of the center frequency is less than a predetermined threshold δ:

$$\frac{f_c - \overline{f_c}}{f_c} = \frac{\beta B^2 x}{2 f_c} < \delta \tag{33}$$

which leads to the following limitation for B:

$$B < \sqrt{\frac{2 f_c \delta}{\beta x}}. \tag{34}$$

For $y = 2$, it can be shown that the new spectrum of the attenuated pulse becomes:

$$S_1(f) = \overline{A} e^{-\frac{(f-\overline{f_c})^2}{(B/\sqrt{1+\beta B^2 x})^2}} \tag{35}$$

where $\overline{A}$ is another new amplitude independent of frequency, and $\overline{f_c}$ is the new down-shifted center frequency:

$$\overline{f_c} = \frac{f_c}{1 + \beta B^2 x}. \tag{36}$$

In this case, the narrowband conditions become:

$$\frac{f_c - \overline{f_c}}{f_c} = 1 - \frac{1}{1 + \beta B^2 x} < \delta \tag{37}$$

and

$$B < \sqrt{\frac{\delta}{(1-\delta)\beta x}}. \tag{38}$$

When $1 < y < 2$, the down-shift in the center frequency is more difficult to formulate. Because we only need to know the upper limit rather than a precise value for B, the following simplified procedure may be used to determine a suitable upper limit for B. If $y < 1.5$, one may fit the attenuation function with a straight line and then use the resulted β value and (34) to determine the upper limit of B. If $y \geq 1.5$, one may fit the attenuation function with a quadratic function and then use the resulted β value and (38) to determine the upper limit for B. Finally, from the values of B, f_L and f_H, the number of band can be determined:

$$n \geq 1 + \frac{f_H - f_L}{B}. \tag{39}$$

As an example, we will choose the parameter B for the bandpass filters used in this study. We first set the threshold as $\delta = 5\%$. For the Plexiglas phantom, $y = 1$ and $\beta = 0.9/8.686 = 0.104$ Np/(MHz cm), and $x = 8.0$ cm. If we let $f_c = 3.0$ MHz, the narrowband criterion based on (34) is $B < 0.6$ MHz. For the ATS phantom, $y \cong 2$, $\beta = 0.2/8.686 = 0.023$ Np/(MHz^{y}cm), and $x = 8.0$ cm. The narrowband criterion based on (38) is $B < 0.53$ MHz. To meet both conditions, a $B = 0.5$ MHz is used in this study. For the wideband transducer (Panametrics V309), $f_L = 0.5$ MHz and $f_H = 5.5$ MHz. The total number of the bandpass filters is 11, according to (39). For the narrowband transducer (Panametrics A382), $f_L = 1.5$ MHz and $f_H = 4.5$ MHz. The total number of the bandpass filters is 7.

Despite the conceptual simplicity, the proposed method accurately predicts the change in the waveform of a pulse transmitting through a layer of lossy medium. When the medium (Plexiglas) has a linear-with-frequency attenuation, Table I indicates that the effects of dispersion, in terms of phase lag and relative time delay, are significant. Fig. 8 shows that the transmitted pulse predicted by the model [Fig. 8(b)] accurately resembles the actually measured pulse [Fig. 8(a)] with a normalized rms error of 6.8%. On the other hand, if the dispersion is ignored, the error is increased to 35.7% [Fig. 8(c)]. Similar results also are obtained when a narrowband transducer is used (Fig. 11): a normalized rms error of 5.7% for the dispersive model and an error of 20.3% for the nondispersive model. These observations, which are consistent with the results reported by Kuc [3], indicate that, although the magnitude of dispersion is very small, its effect in changing the waveform of a propagating pulse is significant.

The ATS phantom has an attenuation which is nearly a quadratic function of frequency ($y = 1.98$). As shown in Table II, the time causal model predicts negligible effects of dispersion while the nearly local model predicts significant effects of dispersion. Because the two models predict significantly different dispersion effects, the transmitted pulses simulated by the two models are expected to have significantly different waveforms. Figs. 10 and 12 indeed show these differences. When compared with the measured pulses, the normalized rms errors of the pulses predicted

by the time causal model are 6.2% for the wideband transducer and 8.8% for the narrowband transducer, respectively. The corresponding errors produced by the nearly local modes are 30.9% and 21.1%, respectively. These results suggest that the time casual model is more accurate than the nearly local model in predicting dispersion when the attenuation function is nearly a quadratic function of frequency.

In the literature, experimental verification of the nearly local model has been reported by two groups. O'Donnell *et al.* [11] measured the attenuation and sound velocities of a solution of $CoSO_4$ (1 Mole/L) as well as of polyethylene over the frequency range of 1 to 10 MHz and showed excellent agreement between the measured and predicted dispersion. In these experiments, the attenuation of the tested materials was found to have a nearly linear frequency dependence. More recently, Lee *et al.* [18] used an improved method to measure the attenuation and used a method developed by Sachse and Pao to measure the dispersion. They then used a pair of equations derived from the nearly local model to predict the dispersion from the measured attenuation, and *vice versa*. Although the specimens they used (loaded and unloaded polyurethane) have an attenuation which is significantly nonlinear with frequency ($y \cong 1.7$), their results showed a good agreement between the measured and the predicted values over the frequency range of 0.5 to 5.0 MHz. On the other hand, based on the data reported by Zeqiri for the measurements of the attenuation and dispersion of castor oil ($y = 1.66$) and Dow Corning 710 silicone fluid ($y = 1.79$), Szabo [13] showed that the predicted dispersions using the time casual model are closer to the measured values than that predicted by the nearly local model. The discrepancy between the results reported by Lee *et al.* [18] and Szabo [13] may originate from the fact that the magnitude of dispersion is very small and, therefore, is difficult to measure precisely. Consequently, it may be difficult to examine the accuracy of the model by directly measuring the dispersion. On the other hand, the method presented in this paper only requires the measurements of two pulses: a pulse transmitted through a water path and a pulse transmitted through a specimen. From the two pulses, the attenuation of the specimen can be determined accurately [18]. The same pulses also are used to examine the accuracy of the model prediction. Because no separate measurement of dispersion is needed, the associated uncertainty is eliminated. Consequently, the proposed method may provide a more sensitive means for the comparison of different models.

References

[1] W. Sachse and Y. H. Pao, "On the determination of phase and group velocities of dispersive waves in solids," *J. Appl. Phys.*, vol. 49, pp. 4320–4327, 1978.

[2] K. V. Gurumurthy and R. M. Arthur, "A dispersive model for the propagation of ultrasound in soft tissue," *Ultrason. Imaging*, pp. 355–377, 1982.

[3] R. Kuc, "Modeling acoustic attenuation of soft tissue with a minimum-phase filter," *Ultrason. Imaging*, pp. 24–36, 1984.

[4] S. A. Goss, R. L. Johnston, and F. Dunn, "Compilation of empirical ultrasonic properties of mammalian tissues. II," *J. Acoust. Soc. Amer.*, vol. 68, pp. 93–108, 1980.

[5] P. N. T. Wells, "Review: Absorption and dispersion of ultrasound in biological tissue," *Ultrason. Med. Biol.*, vol. 1, pp. 369–376, 1975.

[6] C. R. Hill, "Ultrasonic attenuation and scattering by tissues," in *Handbook of Clinical Ultrasound*. New York: Wiley, 1978, pp. 91–98.

[7] A. C. Kak and K. A. Dines, "Signal processing of broadband pulsed ultrasound: measurement of attenuation of soft biological tissues," *IEEE Trans. Biomed. Eng.*, vol. BME-25, pp. 321–344, 1978.

[8] A. Papoulis, *The Fourier Integral and Its Applications*. New York: McGraw-Hill, 1962, pp. 120–143, pp. 192–217.

[9] J. C. Bamber and C. R. Hill, "Acoustic properties of normal and cancerous human liver—I. Dependence on pathological condition," *Ultrason. Med. Biol.*, vol. 7, pp. 121–133, 1981.

[10] P. A. Narayana and J. Ophir, "On the validity of the linear approximation in the parametric measurement of attenuation in tissues," *Ultrason. Med. Biol.*, vol. 9, pp. 357–361, 1983.

[11] M. O'Donnell, E. T. Jaynes, and J. G. Miller, "Kramers-Kronig relationship between ultrasonic attenuation and phase velocity," *J. Acoust. Soc. Amer.*, vol. 69, pp. 696–701, 1981.

[12] T. L. Szabo, "Time domain wave equations for lossy media obeying a frequency power law," *J. Acoust. Soc. Amer.*, vol. 96, pp. 491–500, 1994.

[13] ——, "Causal theories and data for acoustic attenuation obeying a frequency power law," *J. Acoust. Soc. Amer.*, vol. 97, pp. 14–24, 1995.

[14] R. de L. Kronig, "On the theory of dispersion of x-rays," *J. Opt. Soc. Amer.*, vol. 12, pp. 547–557, 1926.

[15] R. L. Weaver and Y. H. Pao, "Dispersion relations for linear wave propagation in homogeneous and inhomogeneous media," *J. Math. Phys.*, vol. 22, pp. 1909–1918, 1981.

[16] J. S. Toll, "Causality and the dispersion relation: logical foundations," *Phys. Rev.*, vol. 104, pp. 1760–1770, 1956.

[17] H. M. Nussenzveig, *Causality and Dispersion Relations*. New York: Academic, 1972.

[18] C. C. Lee, M. Lahham, and B. G. Martin, "Experimental verification of the Kramers-Kronig relationship for acoustic waves," *IEEE Trans. Ultrason., Ferroelect., Freq. Contr.*, vol. 37, pp. 286–294, 1990.

[19] T. Önsay and A. G. Haddow, "Wavelet transform analysis of transient wave propagation in a dispersive medium," *J. Acoust. Soc. Amer.*vol. 95, pp. 1441–1449, 1994.

Ping He (M'85) received the B.S. degree in physics in 1968 from Fudan University, Shanghai, China, and the M.S. and Ph.D. degrees in biomedical engineering in 1981 and 1984, respectively, from Drexel University, Philadelphia, PA.

He was a Research Fellow in Biodynamic Research Unit, Mayo Clinic, from 1984 to 1985, where he worked on ultrasonic tissue characterization. Since 1985, he has been with the Department of Biomedical and Human Factors Engineering, where he is currently an associate professor.

Dr. He's research interests are in medical imaging, biological signal processing, and bioinstrumentation. He is a member of IEEE, AIUM, and ASEE.